Equilibrium self-assembly of small RNA viruses

R. F. Bruinsma,[1,2] M. Comas-Garcia,[3] R. F. Garmann,[4] and A. Y. Grosberg[5]

[1]*Department of Physics and Astronomy, University of California, Los Angeles, California 90095, USA*

[2]*Department of Chemistry and Biochemistry, University of California, Los Angeles, California 90095, USA*

[3]*HIV Dynamics and Replication Program, National Cancer Institute, Frederick National Laboratory for Cancer Research, Frederick, Maryland 21702*

[4]*School of Engineering and Applied Sciences, Harvard University, Cambridge, Massachusetts 02138, USA*

[5]*Department of Physics and Center for Soft Matter Research, New York University, 4 Washington Place, New York, New York 10003, USA*

(Received 4 May 2015; revised manuscript received 8 December 2015; published 9 March 2016)

We propose a description for the quasiequilibrium self-assembly of small, single-stranded (ss) RNA viruses whose capsid proteins (CPs) have flexible, positively charged, disordered tails that associate with the negatively charged RNA genome molecules. We describe the assembly of such viruses as the interplay between two coupled phase-transition-like events: the formation of the protein shell (the capsid) by CPs and the condensation of a large ss viral RNA molecule. Electrostatic repulsion between the CPs competes with attractive hydrophobic interactions and attractive interaction between neutralized RNA segments mediated by the tail groups. An assembly diagram is derived in terms of the strength of attractive interactions between CPs and between CPs and the RNA molecules. It is compared with the results of recent studies of viral assembly. We demonstrate that the conventional theory of self-assembly, which does describe the assembly of *empty* capsids, is in general not applicable to the self-assembly of RNA-encapsidating virions.

DOI: 10.1103/PhysRevE.93.032405

I. INTRODUCTION

A. Self-assembly of small RNA viruses

Assembly is a key part of the life cycle of a virus. During assembly, structural proteins and genome molecules produced inside an infected cell combine to form virus particles ("virions"). Remarkably, many small viruses with a single-stranded (ss) RNA genome ("vRNA") will assemble under laboratory conditions in solutions that contain the protein and genome molecular components of the virus [1,2]. Figure 1 shows a reconstruction [3] of the Flock House Virus (FHV), an example of a small ssRNA virus [4]. The icosahedral shell, or "capsid," has an inner radius R_c of about 10 nm and a thickness of about 3 nm. It is composed of 180 identical proteins (CPs). In the Caspar-Klug classification of viral capsids, icosahedral shells composed of 180 subunits are known as "$T = 3$" shells.

The genome of a $T = 3$ virus encodes minimally two proteins: the capsid protein and an RNA-dependent RNA polymerase, together about 4000 bases. A 10-nm radius spherical volume can accommodate about 5000 RNA bases in the form of a (hydrated) crystal of duplex RNA. The density of the minimal RNA genome is thus not far below that of the hydrated RNA crystal form (in some cases the density of the packaged RNA material even *exceeds* that of the crystal form [5,6]). The dimensions of ss RNA genome molecules in solution are hard to measure, but the combined evidence from small-angle x-ray scattering, cryo-EM, and fluorescence measurements indicates that vRNA molecules are swollen in physiological solutions. For example, the hydrodynamic radius of the vRNA molecules of the MS2 virus has been estimated to be about 14 nm [7] whereas R_c is about 11 nm for MS2. Genome encapsidation thus requires a significant level of compression of the vRNA molecules [8].

Viral self-assembly is driven by the competition between repulsive and attractive macromolecular interactions. It is well known that specific affinities—which involve stem-loop and tRNA-like motifs of the native vRNA molecules that bind preferentially to the viral CPs in question—significantly speed up assembly kinetics and allow for assembly at lower concentrations of the components. Nevertheless, self-assembly studies of CPs with non-native RNA molecules (e.g., [9]) indicate that generic interactions are in general capable of packaging ssRNA molecules in the absence of specific CP-RNA affinities, albeit with reduced yield. For example, the viruslike particle shown in Fig. 1 packages non-native ssRNA material. This article will focus exclusively on viral self-assembly driven by generic interactions.

Among the generic interactions, *electrostatics* plays a central role. The CPs of $T = 3$ ssRNA viruses typically—but not always—have a negatively charged "head group" and a positively charged "tail group" (see Fig. 2). The pH-dependent negative charge $-eZ_h$ of the head group is located mostly on the part of the CP that faces the capsid exterior, while the pH-independent positive charge $+eZ_t$ of the tail group faces the capsid interior. Typically, $Z_h \sim Z_t \sim 10$. The net charge of the CPs of the cowpea chlorotic mottle virus (CCMV)—a self-assembling $T = 3$ ssRNA virus whose assembly process has been particularly well studied—is negative under physiological conditions but if the pH is reduced then the sign changes around pH $\simeq 3.6$ [10], the isoelectric point [11]. The charge distribution of CPs that are part of a capsid has a dipolar component that remains very large—of the order of 10^3 Debye—even at the isoelectric point. If the characteristic energy scale of the electrostatic repulsion between CPs in a 0.1-M salt environment is estimated by Debye-Hückel (DH) theory, then values in the range of $10k_BT$ or more are found.

The positively charged CP tail groups have an electrostatic affinity for the negatively charged RNA nucleotides. Evidence is provided by the fact that the strength of the affinity varies inversely with the ionic strength of the solution [12]. Measured dissociation constants [13] for CP/RNA association binding give binding energies in the range of $15k_BT$. It should be noted that the CP/vRNA binding affinity can have important contributions coming from correlation effects [14].

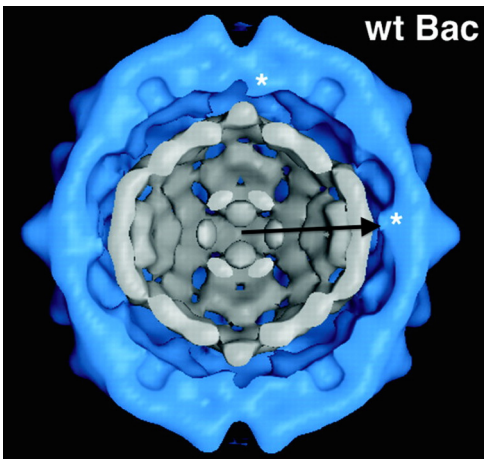

FIG. 1. X-ray reconstruction of a cross section of a T=3 viruslike particle (from Ref. [3]). The capsid is composed of 180 identical copies of Flock House Virus capsid proteins ("wild-type" or wt) arranged in an icosahedral shell (outer layer). The encapsidated RNA material is nonviral, so there are no specific protein-RNA interactions. Only the part of the RNA material that has icosahedral symmetry is shown. The radius of the condensed RNA globule, indicated by an arrow, is about 10 nm. The stars indicate twofold close contacts between the enclosed RNA globule and the capsid. The image is reproduced, with permission, from Ref. [3] [copyright (2004) American Society of Microbiology.].

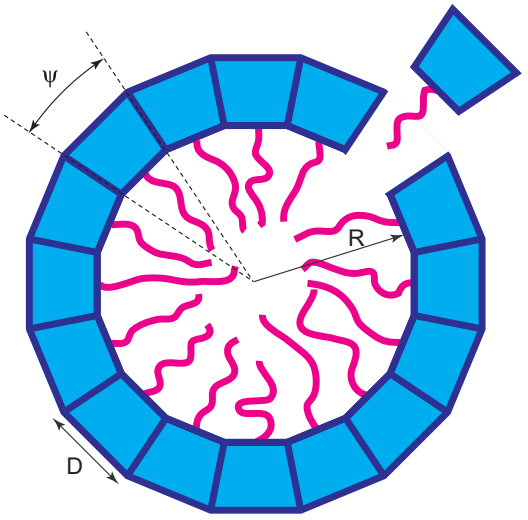

FIG. 2. Schematic cross section of a small ssRNA viral capsid. The positively charged tail groups of the capsid proteins extend inward where they can associate with sections of the negatively charged branched RNA molecules (not shown). The angle ψ is the relative angle between the normals of adjacent capsid proteins. For an inner radius R of about 10 nm and a characteristic capsid protein (CP) dimension D of about 3 nm $\psi \simeq D/R \approx 0.3$ radians. The figure is roughly to scale for a T=3 virus.

Numerical simulations [15,16] report that the electrostatic affinity involves *counterion release*. The importance of CP-RNA electrostatic interactions is manifested by the fact that the amount of vRNA that is packaged by a small ssRNA virus is a linear function of the net positive tail charge [17].

Importantly, neutralization of the ssRNA material by the positive CP tail charges is *incomplete*: the interior of a CCMV virion has a large residual macroion charge in the range of $-10^3 e$. This disparity between the CP tail charge and the vRNA charge is a form of "overcharging," a fundamental issue in the theory of the electrostatics of macroions [18–22]. Deviations from macroion charge neutrality in aqueous solutions are attributed to constraints and/or correlations that prevent matching of the positive and negative charges. In the context of viral assembly, overcharging was attributed by Hu *et al.* [14] to the structure of the CP tail group/RNA association and to Manning condensation by Belyi *et al.* [17].

The repulsive electrostatic interactions between CPs, which inhibit capsid assembly, compete with highly directional CP-CP "pairing" attraction [23]. This attraction is provided by a combination of attraction between complementary hydrophobic patches across CP-CP interfaces and pH-dependent proton-mediated pairing interactions between carboxylate groups on residues of adjacent CPs facing each other ("Caspar pairing" [24]). For capsid assembly to take place, the strength of the attractive interactions between CPs must exceed that of repulsive electrostatic interactions, so it should also be in the range of $10 k_B T$. The competition between the attractive pairing interactions with the salt and pH-dependent electrostatic repulsion is illustrated by assembly diagrams of aqueous solutions of CCMV CPs (but no RNA) with the pH and ionic strength levels as the thermodynamic variables [25,26]. Under conditions of high ionic strength and reduced pH—which means increased attraction—empty capsids assemble spontaneously. This does not happen under conditions of neutral acidity when the negative charge of the CP head groups apparently is just large enough to overcome the attractive interactions.

The assembly of RNA-containing virions is normally described in terms of *kinetic pathways* (e.g., [27]). Numerical studies of simple models for virion assembly [28] show two distinct pathways. If the net CP-CP attraction is large compared to the CP-RNA binding energy then assembly proceeds via a classical nucleation-and-growth pathway. If the net CP-CP attraction is small compared to the CP-RNA binding energy then assembly proceeds via a form of collective condensation ("en masse").

B. Equilibrium self-assembly of virions

This article was motivated by a recent series of self-assembly experiments of CCMV virions carried out under a protocol that maintained, as closely as possible, thermodynamic equilibrium during assembly (e.g., [9]). Equilibrium thermodynamics has already been extensively applied to the self-assembly of *empty* capsids [29] (see also Supplemental Material, Sec. IV [30]). According to equilibrium thermodynamics, the onset of capsid assembly as a function of the solution concentrations of the molecular components has the character of a *phase transition* in the limit that the number of molecular components per aggregate is large compared to one. The critical CP concentration for this transition, sometimes called the "critical micelle concentration (CMC)" [31] by analogy with the self-assembly of micelles, is determined by the condition that the chemical potential of a CP in solution

is the same as that of a CP that is part of a capsid. The predictions of equilibrium thermodynamics agree well with chromatography studies of the self-assembly of empty capsids of CCMV [29] and other other viruses. The characteristic energy scale for the CP-CP interactions in a CCMV capsid at neutral pH was in the range of just a few k_BT, indicating that the repulsive electrostatic interactions between CPs indeed are closely balanced by the attractive interactions.

Under conditions of neutral pH and physiological salt concentrations, empty CCMV capsids do not form in solutions of CCMV CPs but addition of vRNA molecules leads to virion assembly when the pH is reduced [9]. This stabilization of assembly by the vRNA molecules would seem to be obvious on the basis of straightforward electrostatic considerations: if the positively charged tail groups of the CPs are neutralized by the negatively charged vRNA molecules then this should reduce the electrostatic repulsion with respect to the hydrophobic attraction, and hence trigger assembly. For CCMV at least, this argument is invalid. CCMV CPs whose tails have been removed do *not* assemble under conditions of neutral pH [32]. If neutralization of the tail groups was a sufficient condition for assembly then this should have happened. Next, we already saw that CCMV CPs have a dipolar charge distribution and association of the tail group of a CCMV CP with an ssRNA molecule actually *increases* the total negative charge of the assembly (since Z_h exceeds Z_t at neutral pH) and this strengthens electrostatics repulsion. At the isoelectric point, where $Z_h = Z_t$, two CPs can crudely be treated as oriented electrostatic dipoles. In that case, neutralization of the positive charges of the dipoles *still* increases the net repulsion between two CPs for larger separations. An additional source of attractive interactions clearly is required for vRNA-triggered self-assembly of CCMV virions. This additional source of attraction will be assumed to be the *condensation* of vRNA molecules induced by the CP tail groups, as we will now discuss.

C. Condensation of single-stranded nucleotide chains

It is well known that double-stranded (ds) λ phage B-DNA molecules in aqueous saline solutions condense into rodlike and toroidal aggregates when low concentrations of condensing agents are added to the solution [18,33]. The condensing agents—which can be neutral or positively charged polyvalent ions—generate an effective short-range attraction between dsDNA molecules [34]. When low concentrations of poly-L-Lysine are added to solutions containing plasmid length *single-stranded* DNA (ssDNA) molecules then condensation is observed as well [35,36]. These condensates are in fact, under the same conditions, significantly smaller and more stable then their dsDNA counterparts. They have a disordered, spherical appearance under TEM [35,36] and they tend to aggregate together. Which of these two different modes of condensation prevails is believed to be determined by the *persistence length*. The persistence length of ssDNA chains is roughly a factor 50 smaller than that of ds chains. Numerical simulations of linear homopolymers with self-attraction report that, with increasing persistence length, a structural transformation takes place in the morphology of the condensates from a disordered, spherical globule to an ordered toroidal condensate [37,38].

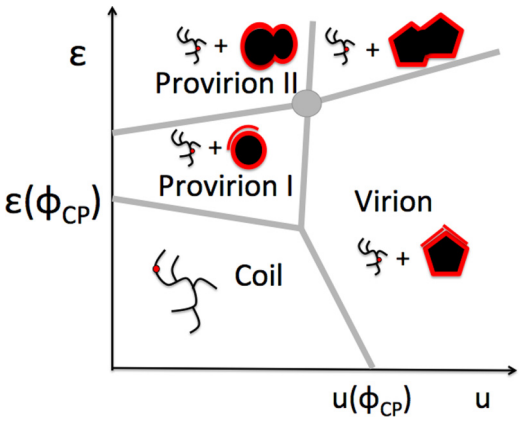

FIG. 3. Equilibrium assembly diagram of a small RNA virus. The vertical axis ε is the binding energy of a capsid protein (CP) to the viral vRNA molecule. The horizontal axis u is the strength of attractive CP/CP pairing interactions. Progressive pH reduction at fixed salinity roughly corresponds to a horizontal path in this diagram. Schematic boundaries between the different regimes, indicated in light gray, are a guide to the eye only.

Disordered spherical condensates appear in solutions of flexible, charged polymers ("polyelectrolytes") to which polyvalent ions have been added as condensing agents. In polymer physics the appearance of such condensates are viewed as an example of the "coil-to-globule" transition [39]. In this article, we will assume that swollen ss vRNA molecules in solution condense via a coil-to-globule transition when condensing agents are added and that CPs in general, and the tail groups in particular, act as the vRNA condensing agents.

D. Equilibrium assembly diagram

Based on the model discussed in the next sections, a schematic equilibrium assembly diagram is obtained shown in Fig. 3. The vertical axis ε is the binding affinity between a CP and a vRNA molecule—including correlation effects [14]—while the horizontal axis u is the strength of attractive CP/CP pairing interactions. If both of these parameters are small compared to k_BT, then the vRNA molecules are swollen and most CPs are free in solution (not shown). Increasing ε increases the number of CPs associated with a vRNA molecule, which effectively reduces the solvent quality. At a threshold $\varepsilon(\phi_{CP})$—which depends on the total CP concentration ϕ_{CP}—the solution *disproportionates* into condensed CP-rich "saturated aggregates" and swollen CP-poor vRNA molecules. Disproportionation is similar to phase separation but without the appearance of phase boundaries [22,40]. Instead, the solution is a uniform mixture of two different populations of aggregate species in thermal equilibrium with each other, as further discussed in Sec. II D. In the present case, one species is composed of swollen vRNA molecules with a small number of associated CPs while the other species is composed of aggregates of condensed vRNA molecules surrounded by a layer of head groups in a liquidlike state ("provirion 1"; see Fig. 4). The CPs are forced out of the interior of a condensed vRNA globule by a combination of *surface tension* of the

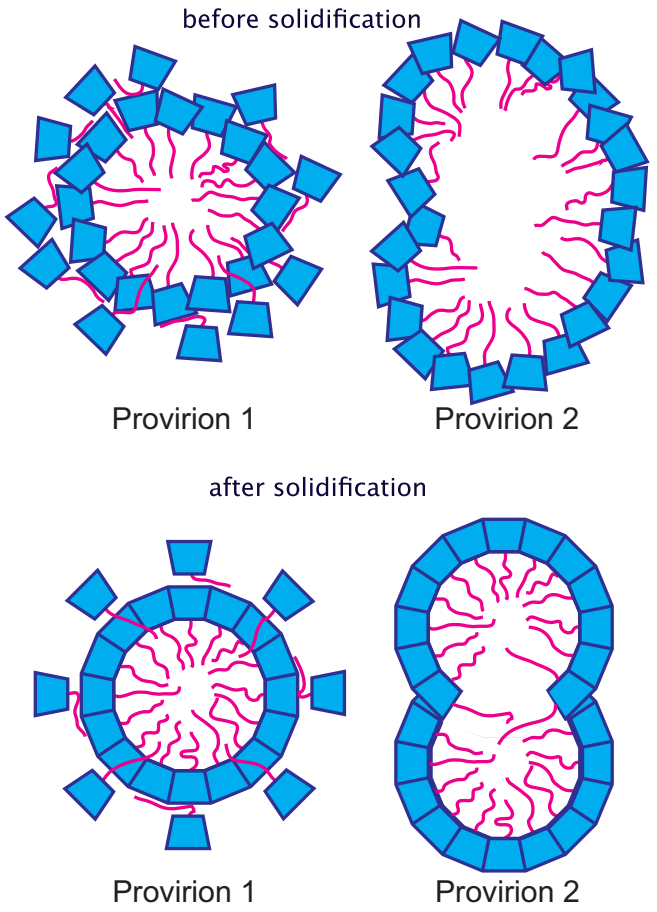

FIG. 4. Provirion 1 and 2 states before (top) and after (bottom) solidification. The number of capsid proteins (CPs) in the first layer of the provirion 1 state whose tails are strongly associated with the RNA molecule(s) is comparable to that of the virion. The interior is negatively charged. The tails of the excess CPs in the second layer have a much weaker association with RNA, either due to the interaction of their tails with the outer side of the first CP layer, or because their tails are forced to squeeze in between the CPs of the first layer to access the RNA. In the provirion 2 state, the number of CPs that are strongly associated with RNA is larger than that of a virion. The tail groups fully neutralize the RNA molecule(s).

globule and angle-dependent pairing attraction between the CPs.

In the provirion 1 state, the condensed, spherical vRNA molecule is surrounded by (roughly) 180 CPs whose tail groups are associated with the vRNA molecule. The tail groups do not neutralize the vRNA molecule so the interior has a net negative macroion charge. Excess CPs either are free in solution or physisorbed on the surface of the provirion. The two populations of bound and free CPs are in thermal equilibrium with each other. If the strength u of the pairing attraction between the CPs is increased then the CPs of the inner layer of the provirion 1 state crystallize out into a $T = 3$ shell of exactly 180 CPs (see Fig. 4). If ε is increased for fixed (small) u, then a second transition is encountered beyond which the CP tail groups neutralize the vRNA molecule. This "provirion 2" state has a significantly larger surface area than the provirion 1 state but a similar volume. It has zero surface tension and is subject to shape fluctuations. Solidification starting from the provirion 2 state is expected to lead to "malformed shells" composed of more than 180 CPs (see Fig. 4). The existence of a provirion 2 state is one of the central predictions of the theory. Provirion 2 aggregates would be a novel application area for the physics of strongly fluctuating interfaces [41], developed originally for surfaces and interfaces composed of amphiphilic molecules. However, the action of the CPs is not due to the competition between the hydrophobic and hydrophilic parts of an amphiphilic molecule but due to the affinity of the positively charged tail groups for the interior of the condensed vRNA molecules and of the negatively charged head groups for the exterior. If provirion 2 particles are indeed found then one might say that CPs act as "amphielectrics."

An essential claim of the proposed model is that virion assembly for larger values of ε does *not* follow the conventional theory of self-assembly [41] and the Law of Mass Action [30] of equilibrium chemical thermodynamics. The key point of the model is that virion assembly will take place from a pre-condensed CP/vRNA aggregate for sufficiently large ε. The CP concentration inside such an aggregate can be very high, even when the CP solution concentration is very low, provided that ε is large enough to offset the low CP solution chemical potential and allow aggregate formation. The final assembly of the virion from this pre-condensed state for increasing u is then independent of the solution CP concentration. In essence, the aggregate acts as a chemical reactor that concentrates the components.

If the strength u of the attractive interactions is increased for $\varepsilon < \varepsilon(\phi_{\rm CP})$, then there is no disproportionation. Instead, virion assembly takes place directly from the swollen coil phase and follows the conventional Law of Mass Action scenario of empty capsid assembly. We speculate—but have not shown—that in terms of assembly kinetics, a direct transition from the coil phase to the virion phase for lower ε obeys the nucleation and growth scenario. In contrast, virion assembly starting from the provirion 1 and 2 states—so for larger ε—is expected to proceed via some form of the "en masse" kinetic scenario. An interesting aspect of the phase diagram of Fig. 4 is the fact that the equilibrium phase diagram includes the provirion I structure as a stable structure. If an assembly experiment would produce a structure like the provorion I, then this would normally be interpreted as a "kinetic trap." That does not mean that there are no kinetically trapped states in the proposed model. If an equilibrium phase diagram includes multiple competing structures separated by first-order transition lines—as is the case for the proposed model—then this only enhances kinetic trapping. The equilibrium assembly of virions requires in general a very fine balance between competing nonspecific interactions.

In Sec. II, we present the simplest version of the model that describes the condensation of vRNA molecules as a coil-to-globule transition induced by CPs. Section III extends the model to include capsid formation deeper in the condensed phase. In the concluding Sec. IV we compare the model with the recent experiments on the equilibrium assembly of CCMV, and discuss experiments that would help to verify (or disprove) the model. We conclude with a discussion of the limitations of the model and how it could be extended further. For the convenience of the reader, a table of symbols used in the paper is provided in the Supplemental Material [30].

II. COIL-TO-GLOBULE TRANSITION

In its simplest form, the model is a variational free energy for a homogeneous CP/RNA aggregate in terms of the radius of gyration R of the aggregate, the maximum ladder distance S (or *MLD*), defined as the maximum number of complementary paired nucleotides separating two points of the RNA molecules [42], and the segment occupation probability x. The latter is defined as the probability that a segment of the vRNA molecule is associated with the tail group of a CP. The variational free energy $F(R,S,x)$ is defined as

$$\beta F(R,S,x) = \frac{R^2}{l^2 S} + \frac{S^2}{N} + V(x)\frac{N^2}{R^3} + W\frac{N^3}{R^6} - \\ -Nx\beta\varepsilon + N[x\ln x + (1-x)\ln(1-x)] \\ +\beta F_{PB}(R), \qquad (2.1)$$

with $\beta = 1/k_B T$. The different terms will be explained in sequence.

A. Coil-to-globule transition of annealed branched polymers

The first four terms constitute together the variational free energy of an *annealed branched homopolymer* in the Flory approximation [43,44]. The branched homopolymer representation for vRNA molecules was developed in Ref. [42] where the secondary structure of vRNA molecules was approximated as a collection of N identical rigid segments of length l connected by freely jointed triple junctions into a treelike structure. Analysis of RNA secondary structures [42] indicates that a reasonable choice for l is about six nucleotides. For a 4000 base vRNA molecule, the number of segments N is then in the range of 10^3 (more details are provided in Supplemental Material, Sec. I [30]). The different possible configurations of the branched polymer represents the different possible secondary structures. Numerical evaluation of the enthalpy of vRNA molecules shows that there is a very large number of secondary structures with enthalpy within $k_B T$ of the ground state [42]. Two examples of treelike structures with the same number of segments ($N = 21$)—but different MLDs (6, respectively, 11)—are shown in Fig. 5.

Returning to Eq. (2.1), the first term is the entropic elastic free energy of a *linear* homopolymer of S segments with a radius of gyration R. The second term is the conformational entropic free energy of an N-segment branched polymer whose MLD equals S. The third and fourth terms represent the interactions between the segments expressed in the form of a virial expansion in powers of the segment density N/R^3. The second-order coefficient V, which has the dimension of volume, is typically of the order of l^3. It can be positive ("good solvent") or negative ("bad solvent"). The coefficient W of the third-order term—which represents the strength of three-body interactions—must be positive to ensure thermodynamic stability. It is typically of the order of l^6. Minimization of the sum of the first four terms with respect to S and R leads to a smooth coil-to-globule condensation transition around $V = 0$. In the good solvent case, the radius of gyration scales with the number of segments N as $R(N) \propto N^{7/13}$, which means that the swollen, or coil, state has a fractal geometry. In the condensed phase, with negative V, the globule size scales as a compact object with $R(N) \propto N^{1/3}$. In either case, the MLD is determined by the radius of gyration through $S(R) \sim (N(R/l)^2)^{1/3}$. It follows that condensation decreases the MLD, thus increasing the amount of branching.

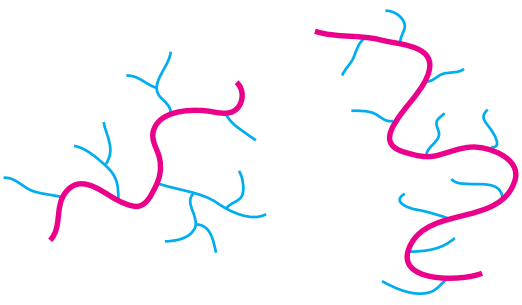

FIG. 5. Different realizations of branched tree structures composed of $N = 21$ segments. The first structure has a maximum ladder distance $S = 6$ while $S = 11$ for the second structures. Both are indicated in red.

B. Mixing entropy

An important feature of the model is the fact that the second virial coefficient $V(x)$ of the branched polymer depends on the probability x that a segment is associated with a CP. In the model, precisely one segment can associate with the tail of one CP so the maximum number of CPs that can associate with the branched polymer equals N. We will call such an $x = 1$ aggregate a "saturated aggregate." Because CP-free vRNA molecules are known to be swollen under conditions of neutral pH and physiological salt concentrations, $V_0 \equiv V(x = 0)$ will be assumed to be positive. On the other hand, in order for the CPs to act as condensing agents for vRNA molecules, $V_1 \equiv V(x = 1)$ should be negative. The model assumes a linear interpolation $V(x) = V_0 - x(V_0 - V_1)$ between these two limits [45].

Returning to Eq. (2.1), the fifth term represents the binding affinity of a CP with a segment while the sixth term is the entropy of distributing Nx different CPs over N different segments.

C. Electrostatic free energy

The last term $F_{\rm PB}$ of the variational free energy is the electrostatic free energy of the aggregate as obtained from Poisson-Boltzmann (PB) theory (see Supplemental Material, Sec. III [30] for a discussion of PB theory in the context of the model). The macroion charge distribution is assumed to be as follows. The tail group is assigned a charge eZ and the head group a charge $-eZ$, with $Z \sim 10$, while the segments of the branched polymer are assigned a negative charge of $-eZ$, so one tail group can neutralize one segment. The total macroion charge of the branched polyelectrolyte molecule equals $-NZ$ independent of the number of associated CPs. These macroions are placed in a monovalent salt solution with ion concentration $2c_s$. In PB theory, the electrostatic free energy of a macroion is determined by the *charging parameter* α, which is defined as the ratio of the effective macroion charge Q^* contained in a certain volume Ω over the number $2c_s\Omega$ of monovalent salt ions in that same volume in the absence of the

macroion charge. The effective macroion charge differs from the bare charge because the monovalent salt ions can condense onto the macroion and thereby diminish the effective charge. Within PB theory, the effective charge per unit length of a highly charged polyelectrolyte molecule equals $-e/l_B$, where l_B is the Bjerrum length defined by $e^2/\varepsilon_0 l_B = k_B T$ with ε_0 the dielectric constant of water. For the present case, the effective charge Q^* of the branched polymer equals $-(e/l_B)N/l$. For a vRNA molecule of 4000 nucleotides confined to a sphere with a radius R of the order of 10 nm, the charging parameter $\alpha = |Q^*|/2\Omega(R)c_s$, with $\Omega(R) = (4/3)\pi R^3$, is of the order of one.

The PB electrostatic free energy of capsid assembly has been extensively discussed (e.g., [46,47]). In the limits of small and large charging parameters it is given by [30]

$$\begin{aligned} \beta F_{\rm PB}(R) &\sim \frac{l^2}{\kappa}\frac{N^2}{R^3} && \alpha(R) \ll 1, \\ \beta F_{\rm PB}(R) &\sim 2Q^* \ln\left(\frac{Q^*}{\Omega(R)c_s}\right) && \alpha(R) \gg 1. \end{aligned} \tag{2.2}$$

Here, $\kappa^2 \equiv 4\pi c_s e^2/(\varepsilon_0 k_B T)$ is the square of the Debye screening parameter. Note that, in the weak-charging limit, $F_{\rm PB}(R)$ has the same form as the second virial term in Eq. (2.1) [48].

D. Phase diagrams

In order to obtain the phase diagram, $F(R,S,x)$ is first minimized with respect to R and S for fixed occupancy x. The resulting free energy $F(x)$ has in general either one minimum or two minima separated by a maximum. For values of x near the maximum, the system is thermodynamically unstable and the solution decomposes into aggregates with different values of x. As the magnitude $-V_1$ of the negative second virial coefficient is reduced, then the two minima of $F(x)$ approach each other and merge at a critical value V_c. Define $\langle x\rangle$ to be the mean occupancy, i.e., the average of the microscopic variable x over all aggregates in solution. The mean occupancy is determined by the condition of phase equilibrium between CPs that are associated with the branched polyelectrolyte and those that are free in solution. Equating the chemical potential μ of the CPs in solution to the derivative $\frac{\partial F(x)}{N\partial x}$ of the free energy of CP that is part of an aggregate with respect to the number xN of CPs leads to a condition from which the mean occupancy $\langle x\rangle$ can be obtained by a common-tangent construction.

1. Two types of disproportionation phase diagrams

The shape of the resulting phase diagram depends crucially on the charging parameter. For the weak-charging regime and $\beta\varepsilon$ large compared to one, the phase diagram is shown in Fig. 6. In this regime, the mean occupancy $\langle x\rangle$ can be equated to the macroscopic CP to RNA concentration ratio $X = \phi_{\rm CP}/N\phi_{\rm RNA}$, normalized so $X = 1$ corresponds to the concentration ratio of a saturated aggregate. We will assume that X is less than or equal to one (as is the case for the experiments discussed in the conclusion).

The horizontal axis is the CP to vRNA concentration ratio and the vertical axis is the negative of the second virial coefficient V_1 of a saturated aggregate. The solid dot indicates a critical point—with $V_1 = V_c$ that marks the onset of the phase decomposition [49]. The interval of phase decomposition widens as the strength of the negative second virial coefficient increases.

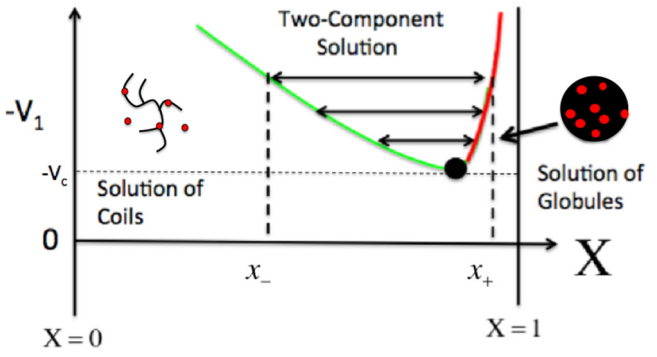

FIG. 6. Disproportionation of a mixture of CP proteins and RNA molecules for large binding affinities ε (weak-charging regime). The horizontal axis is the CP to vRNA concentration ratio X. The vertical axis $-V_1$ is minus the effective second virial coefficient of a saturated globule. If $-V_1$ exceeds the critical value $-V_c$ then phase decomposition takes place for mixing ratios in the interval $x_- < X < x_+$. The solid dot indicates a critical point.

This phase diagram closely resembles that of the *phase separation* of a polymer solution into dense and dilute phases when the solvent quality changes from good to bad [39]. There is, however, an important difference in terms of interpretation. If the solvent quality is reduced in a polymer solution then the formation of globules typically induces macroscopic phase separation, as is the case when condensing agents are added to a solution containing ss DNA molecules [35,36]. However, macroscopic phase separation does not (and should not!) occur during viral assembly. The reason is that the aggregates remain highly charged since the CPs, acting as the condensing agents, are charge neutral (at least in the model). From this it follows that the CP-rich and CP-poor moieties in the two-phase region of the phase diagram remain mixed together in a dispersed state. Decomposition without macroscopic phase separation is in fact well known from the literature on complexation of oppositely charged polyelectrolytes as disproportionation [22,40] and we have adopted this usage.

The phase diagram in the strong-charging regime is shown in Fig. 7. The critical point has been replaced by a sharp,

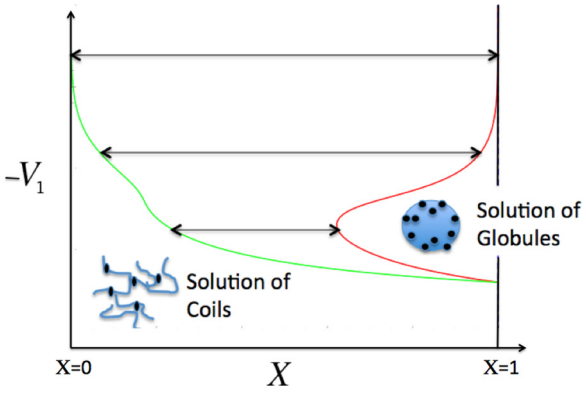

FIG. 7. Same as Fig. 6 but now in the strong-charging regime.

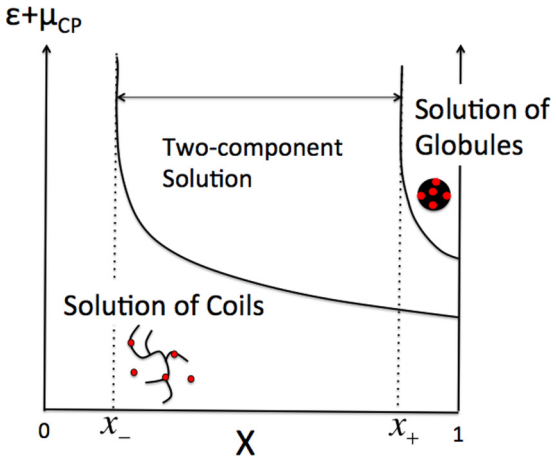

FIG. 8. Phase decomposition for fixed second virial coefficient V_1. The vertical axis is the sum of the CP to RNA binding affinity ε plus $\mu_{\rm CP}$ where $\beta\mu_{\rm CP} = \ln(\phi_{\rm CP}/c_0)$. Here, $\phi_{\rm CP}$ is the total CP concentration and c_0 the CP concentration for a densely packed array of capsids. The horizontal axis is the CP to RNA mixing ratio X. The boundaries of decomposition x_- and x_+ for large binding affinities are those shown in Fig. 6.

first-order coil-to-globule transition along the saturated globule line $X = 1$. For X less than one, this transition broadens out into a wedge of phase decomposition, much like any phase transition of a single-component material tends to broaden into a phase-coexistence interval when impurities are mixed in. Note the surprising "re-entrance": if V_1 is increased starting from the coil phase for X near one then disproportionation appears, disappears, and then reappears.

2. *Coil-to-globule transition*

As the binding affinity is reduced, the phase diagram becomes dependent not just on the concentration ratio but also on the total concentrations. This is shown in Fig. 8, which displays the dependence of the width of the two-phase region on ε and the CP concentration $\phi_{\rm CP}$ for the case that $-V_1$ is larger than the critical value $-V_c$ (see Fig. 8). The vertical axis is the sum of the CP to RNA binding affinity ε and $\mu_{\rm CP}$ with $\beta\mu_{\rm CP} = \ln(\phi_{\rm CP}/c_0)$. Here, $\phi_{\rm CP}$ is the total CP concentration and c_0 is the CP concentration for a densely packed array of capsids. For $X \simeq 1$ the aggregate is in the condensed globule state for larger $\beta\varepsilon$. When $\beta\varepsilon$ is reduced the solution decomposes into one moiety with aggregates whose occupancy $x = x_+$ is close to one (the globule state) and one moiety whose occupancy x_- close to zero (the coil state). For sufficiently low $\beta\varepsilon$, the system is again in a one-phase region, but now with most CPs in solution and with the vRNA molecules in the coil state. The coil-to-globule transition is smeared out as a function of $\beta\mu_{\rm CP} = \ln(\phi_{\rm CP}/c_0)$ because $\mu_{\rm CP}$ is not the true CP chemical potential [30]. For large ε/k_BT, disproportionation is determined only by the concentration ratio X, as we saw earlier.

E. Surface segregation

As $-V_1$ increases, the system enters deeper into the condensed phase. A CP-RNA aggregate can no longer be treated as uniform when this happens. The reason is that the

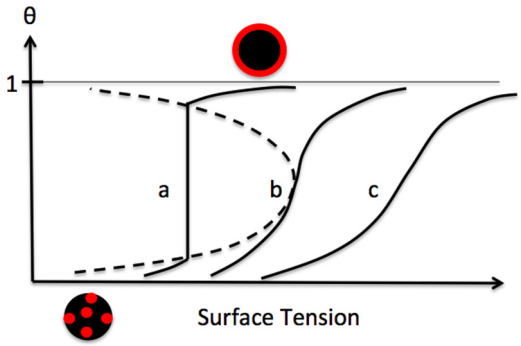

FIG. 9. The fraction of CPs segregated to the surface of a saturated aggregate as a function of the dimensionless surface tension $\beta\gamma_0 D^2$ of the globule. The curves a–c correspond to decreasing attraction u between oriented head groups located on the surface. Curve b corresponds to the critical isotherm.

head groups will segregate out to the surface of the condensate. There are two reasons for this. First, condensed globules have a *surface tension* γ_0 [39] (a simple mean-field argument [30] gives $\beta\gamma_0 \sim V^2/W^{4/3}$). Head groups located in the interior effectively increase the globule surface area. Transferring a head group from the interior to the surface lowers the free energy by an amount $\gamma_0 D^2$, which we estimate to be of the order of $k_BT(D/l)^2$. Next, because head groups transferred to the surface are oriented by the surface—because the tail groups remain bound to the RNA interior—surface segregation also leads to a gain in orientation-dependent attractive interaction between CPs. Figure 9 shows the fraction θ of CPs located on the surface as a function of the dimensionless surface tension $\beta\gamma_0 D^2$ for different values of the strength u of the orientation-dependent attractive interactions between adjacent CPs located on the surface. The curves were obtained using a Langmuir surface-adsorption model with attractive nearest-neighbor interaction for adsorbed particles [30]. The curves marked a–c are lines of fixed strength for the attractive interaction between surface-oriented CPs. Note that the curves resemble the isotherms of the van der Waals gas. If θ is close to one, then the CP layer has the character of a strongly correlated two-dimensional (2D) fluid while for θ close to zero it has the character of a weakly correlated 2D gas. The transition between these regimes can be smooth (case c) or discontinuous (case a). A critical point located on the b isotherm separates the two regimes.

Surface segregation leads to a *geometrical conflict*. Let R be the radius of a condensed globule with no head groups in the interior. If the globule surface area $4\pi R^2$ is less than the area ND^2 of a layer of close-packed CP head groups, then only a fraction of the CPs of a saturated aggregate can be accommodated on the surface. The surface of the vRNA globule of $T = 3$ ssRNA viruses accommodates about 180 CPs while a swollen CCMV vRNA molecule can accommodate about 300 CCMV CPs. One solution to resolve the conflict is for the excess CPs to be expelled into the surrounding solution at the expense of losing an affinity ε per tail group. This corresponds to the provirion 1 state of Sec. I. If ε is increased then breaking the bond between CPs and the vRNA molecule becomes too costly. Instead the surface area of the condensate

can be increased to allow access to the surface for more CPs. This corresponds to the provirion 2 state of Sec. I. In the next section we extend the model to study the competition between the provirion 1 and 2 states, assuming that surface segregation.

III. EXTENDED MODEL: PROVIRION STATES

The extended model is defined by separate free energies for the surface and the interior. The surface free energy area density is defined as

$$\beta f_s(\rho_2) = \rho_2 \ln\left(\frac{\rho_2 D^2}{1-\rho_2 D^2}\right) + B_\psi \rho_2^2 + 2\rho_2 Z \ln\left(\frac{\rho_2 Z l_B}{\kappa}\right) - \beta\epsilon\rho_2. \tag{3.1}$$

The first two terms of Eq. (3.1) constitute the van der Waals free energy density of a two-dimensional system of disklike particles with area density ρ_2 and excluded area D^2. The last two terms are, respectively, the CP electrostatic free energy in the strong-charging limit [30] and the CP-vRNA affinity. The (negative) second virial coefficient B_ψ represents the hydrophobic pairing attraction between surface-segregated CP head groups. It depends on the angle $\psi = D/R$ between the relative orientations of the two axes of adjacent CPs (see Fig. 2) as

$$B_\psi/D^2 = -\exp[\beta u - (\psi - \psi_c)^2/\Delta\psi^2]. \tag{3.2}$$

Here, u is—as before—the binding energy of the pairing attraction, $\Delta\psi$ is the angular range of the pairing attraction, and $\psi_c = D/R_c$ is the relative angle between the CPs of a completed $T = 3$ capsid with $R_c \simeq 10\,nm$ the inner radius of the shell [50].

The surface free energy $F_s = f_s(\rho_2)A$, with A the globule surface area, must be added to the interior free energy $F_b = f_b(\rho_3,x)\Omega$, with $\Omega \simeq (4/3)\pi {R_c}^3$ the globule volume, $\rho_3 = N/\Omega$ the interior segment density, and x the segment occupation probability. The interior free energy density of a highly condense globule also has the van der Waals form:

$$\beta f_b(\rho_3,x) = \rho_3 \ln\left(\frac{\rho_3/\rho_m}{1-\rho_3/\rho_m}\right) - ax\rho_3^2. \tag{3.3}$$

Here, ρ_m is the maximum segment packing density, corresponding to a hydrated crystal of duplex RNA [51]. If we demand that the radius of a close-packed sphere of vRNA segments equals 9 nm then $\rho_m l^3 \simeq 0.37$. The second term describes tail group mediated attractive interaction between RNA segments where $x = \rho_2(A/N)$ is the occupation probability for a vRNA segment to be occupied by a tail group. For provirion states with $\rho_2 D^2 \simeq 1$, the occupancy $x \simeq A/ND^2$ reduces to a dimensionless measure of the surface area. In the limit of small ρ_3, the van der Waals free energy reduces to our earlier virial expansion with a second virial coefficient $V(x) = (1/\rho_m) - ax$ that decreases linearly with the occupation probability [52]. As in Sec. II, the second virial coefficient will be assumed to change sign as a function of x, separating states where the aggregate is in good solvent (for smaller x) or in bad solvent (for larger x). As before, the globule is assumed to have a surface tension $\beta\gamma_0(x) \sim V(x)^2/W^{4/3}$. However, the second virial coefficient $V(x)$ for the surface segregated state in general will be different from that of the uniform globule state.

A. CP-exchange equilibrium and surface phase diagram

The next step is to impose thermodynamic equilibrium of the globule surface and interior, both with respect to each other and with respect to the surrounding solution. The head group surface area density ρ_2 is determined by the condition of exchange or phase equilibrium between CPs located on the globule surface and in the surrounding solution. For simplicity, we will assume in this section that the solution CP chemical potential μ is a fixed quantity. Exchange equilibrium is satisfied if

$$\beta\partial f_s/\partial\rho_2 - a\rho_3 = \beta\mu. \tag{3.4}$$

The second term on the left-hand side is due to the fact that the interior free energy density, through x, also depends on the surface CP density. A surface phase diagram can be obtained in terms of the 2D surface pressure $\Pi_2 = \rho_2 \frac{\partial f(\rho_2)}{\partial \rho_2} - f(\rho_2)$ and the strength $\exp -\beta u$ of the attractive interactions. The surface phase diagram has a line of first-order transitions separating a liquid and a gas phase, as shown in Fig. 10, ending at a critical point (CP) where $\exp\beta u \simeq Z$. In a more complete model, this phase diagram would also contain other phases with, minimally, a solidification line ending at a triple point (TP), where it joins a sublimation line (both marked as dashed lines). The horizontal red line will be discussed below. We will restrict ourselves to the high-density liquid phase with $\rho_2 D^2 \simeq 1$ and $\rho_3/\rho_m \simeq 1$. The solution for Eq. (3.4) corresponding to those condition has a surface pressure $\Pi_2 \sim (\mu + \epsilon)/D^2$ that increases (approximately) linearly with $(\mu + \epsilon)$ [53].

B. Mechanical equilibrium

The next step is to impose *mechanical equilibrium* which requires that the total free energy is minimized with respect to

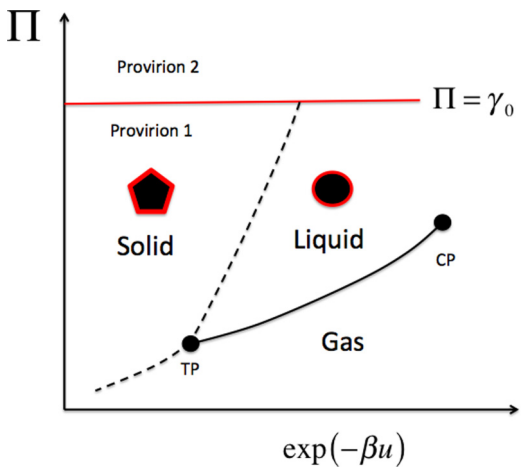

FIG. 10. Phase diagram of the surface layer. (Solid line) Liquid to gas transition, ending at a critical point (CP). (Dashed lines) Solidification and sublimation lines ending at the triple point (TP, not included in the model). The thermodynamic surface tension vanishes along the red line.

ρ_3. This leads to

$$\frac{2(\gamma_0(x)-\Pi_2)}{R}-\frac{K_H}{R_c}\left[\frac{2}{R}-\frac{2}{R_c}\right]^3=\Pi_3(\rho_3). \tag{3.5}$$

Here, $\Pi_3=-\partial F_b/\partial\Omega$ is the three-dimensional (3D) osmotic pressure exerted by the interior on the surface layer. The first term on the left-hand side can be understood by noting that $\gamma=\gamma_0-\Pi(\rho_2)$ is the *thermodynamic surface tension*—defined as $\gamma=\partial F/\partial A$—so $2\gamma/R$ can be interpreted as a *Laplace pressure*. Under conditions of thermodynamic equilibrium, the thermodynamic surface tension is related to the chemical potential by the Gibbs isotherm $d\gamma=-\rho_2 d\mu$ with μ again the chemical potential.

The second term in Eq. (3.5) is a pressure that is generated by the dependence of the second virial coefficient B_ψ on angle, and hence on R. The same term would have been obtained if we had included a *Helfrich bending energy* in the surface energy with mean curvature $2/R$ and spontaneous curvature $2/R_c$ (see also Ref. [54]). Here, $\beta K_H=\exp(\beta u)/\Delta\psi^2$ acts as a dimensionless bending modulus. Equation (3.5) can be extended to nonspherical surfaces, by replacing $2/R$ with the mean curvature. Finally, the pressure $\Pi_3(\rho_3)$ in Eq. (3.5) exerted by the interior on the surface is given by the usual van der Waals equation of state:

$$\beta\Pi_3(\rho_3)=\frac{\rho_3}{1-\rho_3/\rho_m}-a x{\rho_3}^2. \tag{3.6}$$

We will only consider solutions of Eq. (3.5) with $\rho_2 D^2\simeq 1$ and $\rho_3/\rho_m\simeq 1$. The nature of the solution depends in this case on which term dominates the left-hand side of Eq. (3.5).

1. Provirion 1 state

First assume smaller values for $\epsilon+\mu$ and larger values for u so the second term, the Helfrich pressure term, dominates over the Laplace pressure term. The dominant Helfrich energy is minimized if the shell adopts the geometry of a sphere with radius equal to the spontaneous curvature radius (here R_c). The segment occupation probability x can be equated to $x_v=4\pi R_c^2/N D^2$, the occupation probability of an assembled virion (for CCMV, x_v is of the order of 0.6). A significant fraction of the RNA segments are not associated with a tail group in this state, which reflects the geometrical conflict we noted earlier. The second virial coefficient has increased from $V(x=1)$ to $V(x=x_v)$ when x is reduced from a value close to one to x_v. Similarly, the bare surface tension of the globule must be reduced, say to $\gamma_0(x_v)$ If $V(x_v)$ still is negative, like $V(x=1)$, then the RNA material remains in the condensed state. The interior osmotic pressure Π_3 exerted on the shell can be neglected in this case. The thermodynamic surface tension may be positive or negative, depending on the sign of $\gamma_0(x_v)-\Pi_2(\epsilon+\mu)$. Surfaces with a negative surface tension normally are thermodynamically unstable but the Helfrich bending energy can suppress this instability for sufficiently large bending energy. If, on the other hand, the second virial coefficient $V(x_v)$ of the interior is positive then the interior is in a good solvent state and exerts a positive osmotic pressure on the shell. The bare surface tension is zero in this case. The combined pressures $\Pi_3+2\Pi_2(\epsilon+\mu)/R_c$ must be adsorbed by the Helfric bending energy.

2. Provirion 2 state

For increasing $\mu+\epsilon$ the surface pressure Π_2 rises. When $2\Pi_2/R_c$ approaches K_H/R_c^4 in magnitude then the Helfrich bending energy is no longer able to compensate for the surface pressure. The surface area is forced to expand until the occupation probability reaches its maximum value $x=1$. The interior remains condensed since $x=1$ so the interior pressure Π_3 can be set to zero. Because the surface area $A\simeq N D^2$ now exceeds $4\pi(R_c)^2$ the surface cannot remain spherical. By analogy with similar problems in the physics of surfactants [41], we expect that the mean curvature will remain close to $2/R_c$ over sections of the surface that are bounded by lines of negative Gauss curvature where that is not the case.

IV. SUMMARY AND CONCLUSION

In this concluding section, we first compare a number of predictions of the model with the outcome of recent experiments on self-assembly of the CCMV virus. We then discuss predictions of the model that have not yet been tested and conclude with the most important limitations of the model.

A. Comparison with experiment

The most distinctive prediction of the model in terms of experimental tests concerns the *optimal mixing ratio* (OMR), defined as the minimum value of the CP-to-vRNA concentration ratio X for which all of the vRNA molecules are packaged. The OMR has been measured through virion assembly experiments in solutions that contained CCMV CPs and non-CCMV vRNA molecules, using an assembly protocol aimed at maintaining thermodynamic equilibrium [9]. The non-native vRNA molecules had the same length as that of CCMV vRNA molecules. Solutions with a prescribed mixing ratio were first incubated at neutral pH and low salinity, so with weak CP-CP pairing attraction. Cryo-EM images of the solution revealed the formation of virion-sized complexes of CP and RNA with irregular and disordered shapes. RNase digestion assays showed that these disordered complexes did *not* protect the RNA from degradation by RNase so the complexes could not be stable virions. CP-RNA binding was reversible and CPs could exchange between different RNAs [55]. When CP-CP interactions were strengthened by lowering of the pH from 7.2 to 4.5, true virions formed from these structures.

The results of electrophoresis runs for different mixing ratios X [55] are shown in Fig. 11. The far left column shows the case of native CCMV. The far right column shows the case of solutions containing only RNA molecules, which thus move faster than native CCMV virions during gel electrophoresis. For the case of CP to RNA weight ratios w below 6.0, a narrow band moves with a velocity slightly less than that of CCMV virions. The weight rato w is related to the mixing ratio X of the previous sections by $w\simeq 6.0X$ so $w\simeq 6.0$ corresponds to $X\simeq 1.0$. This suggests that aggregates in this band at least resemble the CCMV virion. These labile aggregates could not correspond to the provirion 2 state, since the provirion 2 state is larger than the CCMV virion state, and are candidates for the provirion 1 state.

The faster RNA band has broadened out extending from velocities higher than that of the pure RNA molecule, down

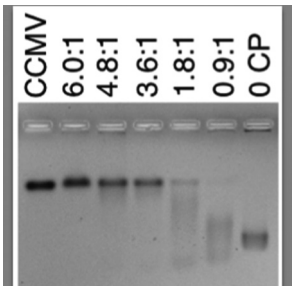

FIG. 11. CP-RNA assembly titrations: gel retardation assays. Shown are 1% agarose gels run at low pH and stained for RNA. At the left is a titration of 3217nt RNA1 molecules of the Brome Mosaic Virus (BMV) with varying amounts of CCMV CP. The value of the CP to RNA weight ratio w is provided at the top of each lane. It ranges from 0 (right-most lane, RNA) to 6:1 (lane second from left). The weight ratio w is related to the mixing ratio X of the text by $w \simeq 6.0X$. The left-most lane shows the position of CCMV virions. From Ref. [9].

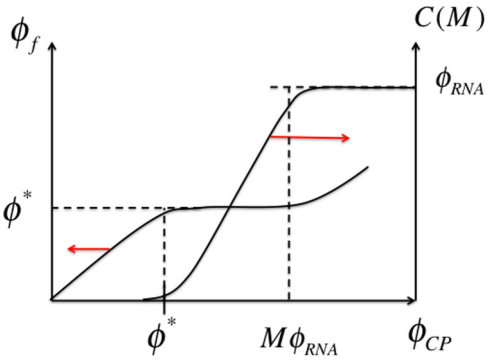

FIG. 12. Dependence of the concentration ϕ_f of free capsid proteins and that of the capsid concentration $C(M)$ on the total protein concentration $\phi_{\rm CP}$ (left vertical axis) according to textbook theory. Capsid assembly starts at the CMC ϕ^* and terminates when the RNA supply has been exhausted at $\phi_{\rm CP} \simeq M\phi_{\rm RNA}$ with M the number of CPs per virion.

to the CCMV-like band. Aggregates in this smeared out band are not packaged when the interaction strength is increased, so X is less than the OMR. If the CP concentration is increased then the broad band disappears around a concentration ratio of about 300 CPs per vRNA molecule. For a positive tail charge of about $+10e$, this corresponds to an OMR of $X = 1$.

This is a striking result. If one would apply textbook self-assembly theory [41] then—by directly minimizing the free energy of a solution of CPs and vRNA molecules in the absence of any CP-induced vRNA condensation—one obtains Fig. 12 [30]. As a function of increasing CP concentration, capsid assembly starts at a CMC, denoted by ϕ^*, which is proportional to the Boltzmann factor for inserting a CP into a virion shell. Beyond ϕ^*, the concentration of free CPs saturates while that of assembled capsids increases linearly with the CP concentration. The increase stops when the supply of vRNA molecules is exhausted, which is the OMR at which (nearly) all vRNA molecules have been packaged. The OMR is thus $X = M/N$, with M the number of CPs of a $T = 3$ shell and N the number of vRNA segments [30].

The value of the OMR predicted by the model follows from Figs. 6–8. These show that the solution should disproportionate into CP-rich globules and CP-poor vRNA molecules. Provided the CP-rich globules are in the provirion 1 state, the globules should transform into virions when the strength u of the CP-CP pairing is increased and the 2D liquid freezes into a $T = 3$ "crystal." The CP-poor swollen vRNA molecules will not be packaged. It follows that, for the model, the OMR is $X = 1$. More generally, the OMR corresponds to charge neutralization of the vRNA molecule by the CP tail groups. Measurement of the OMR is thus a direct way compare the theory proposed in this paper for virion assembly and textbook self-assembly theory.

If one interprets the smeared-out band in Fig. 11 as being produced by CP-poor swollen vRNA globules then there would seem to be agreement between the predictions of the proposed model and experiment and a direct violation of conventional self-assembly theory. It should be recalled here that conventional self-assembly theory works quite well for the assembly of empty capsids. This interpretation can (and should) be questioned. In a solution that is in *complete* thermodynamic equilibrium, each vRNA molecule should fluctuate thermally between all of the allowed configurations. In an electrophoresis experiment that is carried out on a system in full equilibrium, the vRNA molecules should *all* move with an average speed determined by a Boltzmann average over all accessible states, leading to just one single band. Figure 11 indicates that the previous experiments were carried out on time scales shorter than the thermal equilibration time. Now, it seems reasonable to assume that the lifetime of an assembled provirion state is the longest relaxation time of the system. In an electrophoresis experiment carried out on time scales shorter than this relaxation time but longer than any other relaxation time, one should expect a *bimodal distribution* with two narrow bands. The slow band contains provirions and the fast band corresponds to aggregates that interconvert among each other on the time scale of the experiment. A recent assembly study of CCMV with much shorter 500-nt-long RNA fragments reported bimodal distributions for nearly all CP:RNA ratios [56]. The natural interpretation is that for the case of shorter RNA chains the system is closer to thermal equilibrium. Recently, Kler and co-workers found—for the SV40 virus—that titration of a short RNA molecule (less than 0.8 kb) with VP1 indeed gave a bimodal distribution while binding of VP1 to longer RNAs again led to the formation of intermediate species [57]. Bimodal distributions have also been observed in the *in vitro* assembly of Cucumber Mosaic Virus (CMV) [58]. If the size of the vRNA molecule is increased, then provirions that are missing variable amounts of CPs are expected to have relatively long lifetimes. These would show as a smearing of the slow band.

A second distinctive prediction of the model concerns the claim that the CP-tail groups must be effective vRNA condensing agents. If the compression of the vRNA molecule was purely due to the action of the CP head groups—which we argued against in the introduction—then removal of the CP head groups should cause *swelling* of the vRNA molecule, while the model predicts increased condensation. In Refs. [59,60] it was shown that the vRNA molecules of the

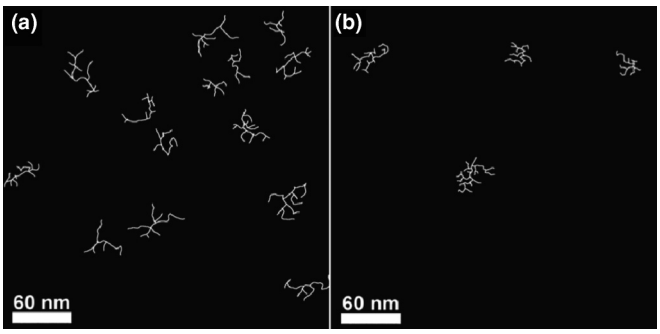

FIG. 13. Cryo-EM images of 2777-nt RNA molecule under assembly conditions (left panel) and assembly conditions with added Mg^{2+} ions. The image is reproduced from Ref. [61] with permission.

$T = 1$ Satellite Tobacco Mosaic Virus (STMV) remained in a fully condensed state after the CP head groups had been enzymatically removed from STMV virions while the tail groups of the CPs remained behind. The resulting particles were thermodynamically very stable. X-ray diffraction studies revealed a tight association between the tail groups and the vRNA molecule [59,60].

Next, in the weak-charging limit, vRNA molecules in good solvent should have a fractal structure with a radius of gyration $R(N)$ that scales with the number of monomers as $N^{1/2}$ while in the strong-charging limit, the molecules should be more linear and extended, and the radius of gyration should be proportional to N. In the condensed state, the radius of gyration should scale as $N^{1/3}$. In either case, the MLD of the vRNA molecule should depend on the radius as $R^{2/3}$, which can be tested experimentally. Gopal and coworkers visualized CCMV RNA 2 (of 2.7 kb) molecules using cryo-electron microscopy [61]. They found that, in a physiological buffer without Mg^{2+}, the RNA molecules adopted highly extended structures with just a few major branches. An example is shown in the left panel of Fig. 13. The appearance of extended vRNA structures suggests the strong-charging regime where the vRNA molecules are effectively stretched by electrostatic repulsion. When the solution concentration of Mg^{++} ions was increased, more compact, spherical shapes appeared with a smaller radius comparable to that of the virus itself as shown in Fig. 13, right panel. These molecules had structures that were significantly more branched than the swollen structures in good solvent. These results seem at least consistent with the simple model of Sec. II.

Has the provirion state been observed microscopically? Figure 14 shows cryo-EM images of 3200-nt RNA molecules when CPs are added to the solution. Figure 14(a) shows the RNA molecule in assembly buffer with added Mg^{2+} in the absence of CPs, as in the previous picture. Note again the elongated arms, indicative of strong electrostatic repulsion. Figure 14(b) shows the same RNA molecule when the CP to RNA mixing ratio X is larger than 0.6. The images were taken at higher pH when the attractive interactions are too weak to support virion assembly. The approximated structure of the RNA molecule is shown in the bottom image. It clearly has undergone a certain degree of additional condensation. The image shows—probably transient—*shell fragments*. If this would be the image of a provirion 1 then the description of the

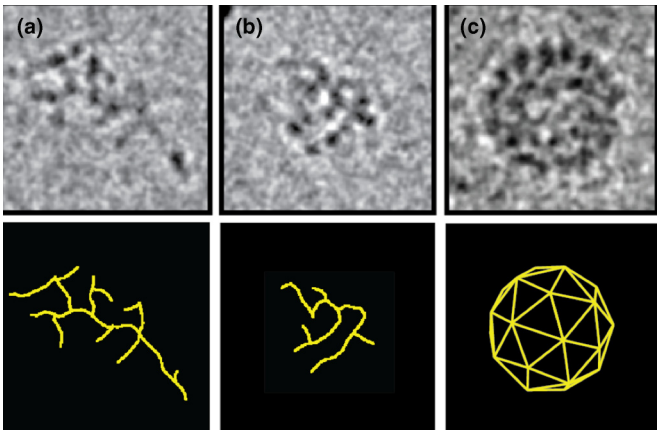

FIG. 14. (Top) Cryo-EM images of 3200-nt RNA during the different stages of assembly. (Bottom) Reconstructions. (a) Shows naked RNA in assembly buffer with Mg^{2+} (see also Fig. 13). (b) Shows the same RNA molecule but decorated with a super-stoichiometric amount of CP at higher pH. Note that the complex is smaller than the naked RNA molecule. Analysis of a large number of cryo-EM images shows that the average size drops from about 37 nm when the RNA is naked to about 32 nm in the provirion state when it is decorated by CP. (c) Shows the formation of capsidlike structures when CP-CP interactions are strengthened by reducing the pH. Reproduced from Ref. [12] with permission from Elsevier.

surface-segregated CPs as a 2D correlated fluid will have to be replaced by a more complex fluctuating state with a statistical distribution over capsid fragments of various size. Figure 14(c) shows the structure of the aggregate when the pH is reduced so the strength of the CP-CP attraction increased. If *this* is an image of a provirion 1 then it would correspond more closely to the description proposed in this paper, although it could also be already a true virion. A key point would be to determine at what pH the shell transforms from a fluid state that is in thermodynamic equilibrium with the surrounding solution to an ordered T=3 capsid with frozen-in CP positions.

B. Tests of the model

We now turn to the predictions of the model that allow future experimental tests of its validity. The existence of a provirion 2 state plays a central role in this respect. According to the general phase diagram (see Fig. 3), increasing the binding affinity ε should lead to a stabilization of provirion 2 state with respect to the provirion 1 state. Increasing ε could be done by systematically increasing the number of positively charged arginine residues on the CP tail groups, as was already done in Ref. [62]. Electron microscopy images of a provirion 2 state should be characterized by strongly fluctuating, nonspherical shapes. Increasing the strength of the CP-CP attraction starting from a provirion 2 state should produce not virions but malformed structures, as in Fig. 5.

Next, reducing ε—for example, by reducing the number of charged residues per tail group—would allow a second experimental test of the proposed model. According to the assembly diagram, for smaller values of $\beta\varepsilon$, assembly as a function of increasing u should proceed without vRNA condensation. According to Fig. 12, the OMR should then be

$X = M/L \simeq 0.6$ (for the case of CCMV at least). Moreover, the fraction of assembled virions measured, as a function of the total CP concentration, should now obey the Law of Mass Action, as is the case for empty capsids but as is not the case in the model if assembly starts from a provirion precursor state.

Another important prediction of the model concerns the presence of either a critical point or a first-order phase transition point in the assembly diagrams (see Figs. 8 and 9), depending on the charging parameter α. This could be tested by repeating the electrophoresis experiments discussed above but now decreasing the magnitude of the negative second virial coefficient $-V_1$. The second virial coeffcient of the CPs could be quantitatively measured separately by thermodynamic studies of CP pair formation in dilute solutions of CPs. Variation of V_1 as a function of pH, salinity, or tail length could then be determined. Measurement of the disproportionation interval—in terms of the mixing ratio X—by gel electrophoresis for different values of V_1 could verify whether the weak or strong-charging regime applied. Recall here the striking prediction of reentrance of the single-phase region in the assembly diagram as a function of $-V_1$ for the strong-charging case.

The experiments discussed above could be repeated for different salt concentrations. Reducing the salinity means increasing the strength of the electrostatic interactions. Studies of the assembly of empty CCMV capsids [1,25,26] reported that at higher CP concentration and lower ionic strength, *multishell structures* form, stabilized by electrostatic interactions [63], where the tail groups of the second layer associate with the head groups of the CP first layer. It has been shown that multilayer shell structures form during assembly of virions with shorter RNA molecules, as shown in Fig. 15 [56]. If the gel-electrophoresis experiments discussed above were repeated at lower salinity, then the excess CPs released in solution would now be expected to remain associated with the CP shell in the form of a second layer (see Figs. 4 and 5). By measuring the number of CPs that remain associated with the virion after assembly—for example, by fluorescent labeling—it could be checked if the number of excess CPs equals the difference between the number of CPs of a saturated aggregate and of a virion (see also Ref. [56]).

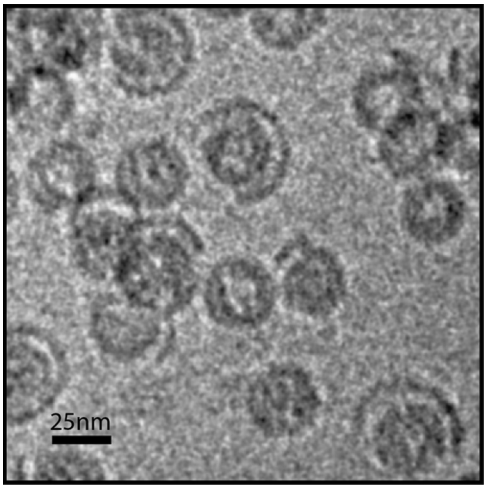

FIG. 15. Cryo-EM images of assembly products of 500-nt RNA. Multishell structures formed with an inner shell that roughly correspond to a $T = 2$ shell and an outer shell that corresponds to an incomplete $T = 3$ shell. Reprinted with permission from [56]. Copyright 2014 American Chemical Society.

C. Overcharging

In the introduction we posed the question why the total positive charge of the CP tail groups of the CPs is not neutralized by the negative charge of the RNA molecule. Recall that overcharging in the context of viral assembly previously has been attributed to the local structure of tail group/RNA association in Ref. [14] and to Manning condensation in Ref. [17]. In the proposed model, overcharging is attributed to correlations between the CP head groups: The homogeneous saturated aggregate, in which the tail groups do neutralize the RNA charge, is "frustrated" by the nonelectrostatic, angle-dependent interactions that drive the formation of the provirion 1 state and the $T = 3$ capsid.

Could experiment resolve questions about the cause of the overcharging? It is possible to enzymatically digest the head groups of a virion [64]. If the proposed explanations of either Refs. [17] or [14] are right, then the macroion overcharge of the remaining RNA/tail-group core particle should remain stable in a solution that contains a modest concentration of tail-group molecules, as it represents a minimum free energy state. On the other hand, in the model proposed here, the core particle should be expected to "soak up" extra tail groups from the surrounding solution causing the overcharge to decrease to zero. Changes of the charge of a core particle could be monitored in an electrophoresis experiment.

This method could also be used to measure the osmotic pressure the RNA/tail-group assembly exerts on the capsid. If this pressure is negative, then the RNA/tail-group core particle ought to contract after enzymatic digestion of the capsid while in the opposite case, it should expand. The radius of the core particles in solution could be measured by AFM, as was already done [64], or in a scattering experiment. By adjusting the osmotic pressure of the surrounding solution until the radius of the core particle would equal the inner radius R_c of the capsid, one could establish the osmotic pressure inside the virion. In the proposed model, the core particle should expand after digestion of the capsid.

D. Limitations of the model

We finish by discussing the limitations of the proposed model. The applicability of the proposed model to the complexity of viral assembly involves both straightforward simplifications that could impair quantitative predictions but which can be improved upon in a systematic fashion, and more "dangerous" assumptions whose failure would compromise the usefulness of the model at a fundamental level.

Straightforward simplifications involve equating the magnitudes of the head group and tail group charges, assuming a linear dependence of the second virial coefficient on occupancy, assuming a Gaussian dependence of the surface second virial coefficient on angle and assuming that the third virial coefficient of a CP/vRNA saturated aggregate does not depend on occupancy. Higher-order terms may

have to be systematically included in the virial expansion. In order to carry out quantitative tests, these assumptions may have to be improved upon. However, we believe—although have not explicitly demonstrated—that none of the key predictions discussed earlier will be affected if the model is generalized.

A more serious limitation of the model concerns the use of mean-field theory. We made the assumption that the interior of a surface-segregated globule is homogeneous. In actuality, because CP tail groups are attached to the surface-segregated CP head groups, neutralization of the negative vRNA charges must be more efficient near the surface of the globule than in the interior. As a result, the macroion charge density will have a radial profile. Mean-field theories allowing spatial variation of the density can be formulated but it would seriously complicate the formalism. Fluctuations around mean-field theory, even one that includes a nontrivial density profile, are neglected as well. As discussed in the conclusion, if the surface of a provirion 1s better described as a collection of transient shell fragments instead of a correlated but uniform fluid then this would be a serious concern for the theory that would not be easy to remedy.

Another "dangerous" limitation of the model is the use of PB theory to describe the electrostatics. It can be shown that the condensation of dsDNA molecules by polyvalent counterions is due to correlation attraction. This effect is beyond PB theory [34] and it is possible—even likely—that the same is true for the condensation of ssRNA molecules. This problem was to some extent "swept under the rug" by including correlation attraction effects as negative contributions to the effective second virial coefficient. The applicability of PB theory can be monitored by measuring the OMR. Serious breakdown of PB theory would be signaled by the appearance of overcharging [65] of saturated aggregates since these would no longer correspond to a state in which the tail groups neutralize the RNA molecules. That would mean that $X = 1$ would not correspond to the OMR. For CCMV at least, that appears not to be the case but it could well be true for other viruses.

A final important limitation of the model is the restriction to equilibrium thermodynamics. The assembly of empty capsids follows—as mentioned—the law of mass action of equilibrium statistical mechanics. In actuality, empty capsids in fact do not disassemble when the CP concentration in solution is reduced back to zero. The final assembly step or steps are quasi-irreversible. This must be true as well for virions or else virions would disassemble in CP free solutions, which is not the case. Kinetic models of empty capsid assembly confirm that a form of the law of mass action survives when only a few number of steps are irreversible [66]. In general, equilibrium models are expected to fail progressively as the number of irreversible assembly steps increases. It is our belief, however, that an understanding viral assembly in general requires understanding viral assembly under conditions of thermal equilibrium.

ACKNOWLEDGMENTS

We wish to thank Chuck Knobler for numerous suggestions, discussions, and readings of the manuscript. We also wish to thank Vinny Manoharan for a critical reading of the draft. We are grateful to Jack Johnson for providing the image used for Fig. 1. We would like to thank as well Michael Hagan and Boris Shklovskii for discussions and comments. R.B. thanks the National Science Foundation (USA) for support under Grant No. DMR-1309423. The work of AYG on this project was supported in part by the National Science Foundation (USA) under Grant No. PHY-1066293. Both A.Y.G. and R.B. wish to thank the Aspen Center for Physics for its hospitality and for hosting a workshop on the physics of viral assembly where some of the work was done.

[1] J. Bancroft, G. Wagner, and C. Bracker, Virology **36**, 146 (1968).
[2] K. W. Adolph and P. Butler, Philos. Trans. R. Soc. London Ser. B **276**, 113 (1976).
[3] M. Tihova, K. Dryden, T. Le, C. Stephen, J. Johnson, M. Yeager, and A. Schneemann, J. Virol. **78**, 2897 (2004).
[4] The viruslike particle was produced in a cell expression system ("wt-Bac") that produces viral proteins, which encapsidate cellular RNA molecules.
[5] J. E. Johnson and R. Rueckert, in *Structural Biology of Viruses*, edited by W. Chiu, R. Burnett, and R. Garcea (Oxford University Press, Oxford, 1997), pp. 269–287.
[6] A. Schneemann, Ann. Rev. Microbiol. **60**, 51 (2006).
[7] A. Borodavka, R. Tuma, and P. G. Stockley, RNA Biol. **10**, 481 (2013).
[8] The compression of the double-stranded DNA genome molecules of phage viruses is carried out by a molecular motor embedded in the viral capsid, but that is not the case for viruses with single-stranded RNA or DNA genomes.
[9] R. Cadena-Nava, M. Comas-Garcia, R. Garmann, A. Rao, C. M. Knobler, and W. M. Gelbart, J. Virol. **86**, 3318 (2012).
[10] J. R. Vega-Acosta, W. M. Gelbart, C. M. Knobler, and J. Ruiz-Garcia, J. Phys. Chem. B **118**, 1984 (2014).
[11] The positive tail group charge derives mainly from arginine and lysine residues. It is not pH dependent because arginine and lysine do not titrate over relevant pH values.
[12] R. F. Garmann, M. Comas-Garcia, A. Gopal, C. M. Knobler, and W. M. Gelbart, J. Mol. Biol. **426**, 1050 (2014).
[13] T. Bayer, L. Booth, S. Knudsen, and A. Ellington, RNA **11**, 1848 (2005).
[14] T. Hu, R. Zhang, and B. I. Shklovskii, Physica A **387**, 3059 (2008).
[15] C. García-García and D. E. Draper, J. Mol. Biol. **331**, 75 (2003).
[16] B. Devkota, A. S. Petrov, S. Lemieux, M. B. Boz, L. Tang, A. Schneemann, J. E. Johnson, and S. C. Harvey, Biopolymers **91**, 530 (2009).
[17] V. A. Belyi and M. Muthukumar, Proc. Natl. Ac. Sci. USA **103**, 17174 (2006).

[18] W. M. Gelbart, R. F. Bruinsma, P. A. Pincus, and A. V. Parsegian, Phys. Today **53**, 38 (2000).
[19] Y. Levin, Rep. Prog. Phys. **65**, 1577 (2002).
[20] A. Y. Grosberg, T. T. Nguyen, and B. I. Shklovskii, Rev. Mod. Phys. **74**, 329 (2002).
[21] A. V. Dobrynin and M. Rubinstein, Progress in Polymer Science **30**, 1049 (2005).
[22] R. Zhang and B. Shklovskii, Physica A **352**, 216 (2005).
[23] W. K. Kegel and P. van der Schoot, Biophys. J. **91**, 1501 (2006).
[24] D. Caspar, Adv. Protein Chem. **18**, 37 (1963).
[25] K. Adolph and P. Butler, J. Mol. Biol. **109**, 345 (1977).
[26] L. Lavelle, M. Gingery, M. Phillips, W. M. Gelbart, C. M. Knobler, R. D. Cadena-Nava, J. R. Vega-Acosta, L. A. Pinedo-Torres, and J. Ruiz-Garcia, J. Phys. Chem. B **113**, 3813 (2009).
[27] D. Endres, M. Miyahara, P. Moisant, and A. Zlotnick, Protein Sci. **14**, 1518 (2005).
[28] O. Elrad and M. Hagan, Phys. Biol. **7**, 045003 (2010).
[29] J. M. Johnson, J. Tang, Y. Nyame, D. Willits, M. J. Young, and A. Zlotnick, Nanoletters **5**, 765 (2005).
[30] See Supplemental Material at http://link.aps.org/supplemental/10.1103/PhysRevE.93.032405 for mathematical details and notation used in the work.
[31] A. McPherson, Bioessays **27**, 447 (2005).
[32] J. Bancroft, G. Hills, and R. Markham, Virology **32**, 354 (1967).
[33] V. A. Bloomfield, Biopolymers **44**, 269 (1997).
[34] N. Grønbech-Jensen, R. J. Mashl, R. F. Bruinsma, and W. M. Gelbart, Phys. Rev. Lett. **78**, 2477 (1997).
[35] M. Molas, R.Bartrons, and J. C. Perales, Biochim. Biophys. Acta **1572**, 37 (2002).
[36] C. Santai, Ph.D thesis, Georgia Institute of Technology, 2006.
[37] H. Noguchi and K. Yoshikawa, J. Chem. Phys. **109**, 5070 (1998).
[38] Z. Ou and M. Muthukumar, J. Chem. Phys. **123**, 074905 (2005).
[39] A. Y. Grosberg and A. R. Khokhlov, *Statistical Physics of Macromolecules* (American Institute of Physics Press, Melville, 1994).
[40] V. A. Kabanov and A. B. Zezin, Pure Appl. Chem. **56**, 343 (1984).
[41] S. Safran, *Statistical Thermodynamics of Surfaces, Interfaces, and Membranes* (Westview Press, Boulder, 2003).
[42] L. Fang, W. Gelbart, and A. Ben-Shaul, J. Chem. Phys. **135**, 155105 (2011).
[43] A. Gutin, A. Grosberg, and E. Shakhnovich, Macromolecules **26**, 1293 (1993).
[44] A. Grosberg, Physics–Uspekhi **40**, 125 (1997).
[45] The bare second virial coefficient V_0 of a branched flexible polyelectrolyte is roughly estimated as l^3. The second virial coefficient V_1 of a saturated aggregate, a more complex quantity, is discussed and estimated in Supplemental Material, Sec. II [30].
[46] A. Siber *et al.*, Phys. Chem. Chem. Phys **14**, 3746 (2012).
[47] Losdorfer-Bozic *et al.*, J. Biol. Phys. **38**, 657 (2012).
[48] Under physiological conditions $1/\kappa$ is of the order of one nanometer.
[49] $(|V_c|)^2/W \sim 1$.
[50] The critical isotherm discussed at the end of the last section is determined by the condition $e^{\beta u} \simeq Z$.
[51] In the provirion states the vRNA density is so large that the virial expansion of Sec. II breaks down.
[52] $W = (1/\rho_m)^2$.
[53] $\beta\Pi_2 D^2 \simeq \beta(\mu+\epsilon) + \exp(\beta u) - 2Z\ln(\frac{Zl_B}{D^2\kappa}) + a\rho_m - \ln(\beta(\mu+\epsilon) + \exp(\beta u) - 2Z\ln(\frac{Zl_B}{D^2\kappa}) + a\rho_m)$.
[54] A. Siber and A. Majdandzic, Phys. Rev. E **80**, 021910 (2009).
[55] M. Comas-Garcia, R. D. Cadena-Nava, A. L. N. Rao, C. M. Knobler, and W. M. Gelbart, J. Virol. **86**, 12271 (2012).
[56] M. Comas-Garcia, R. Garmann, S. Singaram, A. Ben-Shaul, C. M. Knobler, and W. M. Gelbart, J. Phys. Chem. B. **118**, 7510 (2014).
[57] S. Kler, J. C.-Y. Wang, M. Dhason, A. Oppenheim, and A. Zlotnick, ACS Chem. Biology **8**, 2753 (2013).
[58] A. Kobayashi and Y. Ehara, Ann. Phytopathol. Soc. Jpn. **61**, 99 (1995).
[59] Y. G. Kuznetsov, J. J. Dowell, J. A. Gavira, J. D. Ng, and A. McPherson, Nucleic Acids Res. **38**, 8284 (2010).
[60] Y. G. Kuznetsov, S. Daijogo, J. Zhou, B. L. Semler, and A. McPherson, J. Mol. Biol. **347**, 41 (2005).
[61] A. Gopal, Z. H. Zhou, C. M. Knobler, and W. M. Gelbart, RNA **18**, 284 (2012).
[62] R. Garmann, M. Comas-Garcia, M. Koay, J. Cornelissen, C. M. Knobler, and W. M. Gelbart, J. Virol. **88**, 10472 (2014).
[63] P. Prinsen, P. van der Schoot, W. M. Gelbart, and C. M. Knobler, J. Phys. Chem. B **114**, 5522 (2010).
[64] J. Day, Y. G. Kuznetsov, S. B. Larson, A. Greenwood, and A. McPherson, Biophys. J. **80**, 2364 (2001).
[65] T. Nguyen and B. Shklovskii, Physica A **293**, 324 (2010).
[66] A. Morozov, R. Bruinsma, and J. Rudnick, J. Chem. Phys. **131**, 155101 (2009).